Phase Transitions, Phase Coexistence, and Piezoelectric Switching Behavior in Highly Strained $BiFeO_3$ Films

*C. Beekman, W. Siemons, T. Z. Ward, M. Chi, J. Howe, M. D. Biegalski, N. Balke, P. Maksymovych, A. K. Farrar, J. B. Romero, P. Gao, X. Q. Pan, D. A. Tenne, and H. M. Christen**

The multiferroic perovskite $BiFeO_3$ has recently become the subject of intense investigation due to its intriguing coexistence of structural polymorphs in highly-strained epitaxial films that show remarkable stripe-like domain patterns.[1–3] The ferroelectric polarization of the strain-stabilized, highly distorted phase has been predicted[4,5] and experimentally confirmed[6] to reach a value higher than any other perovskite (≈150 μC/cm^2), all while being an environmentally benign lead-free material. By studying $BiFeO_3$ films grown on $LaAlO_3$ substrates and comparing results from temperature-dependent measurements including X-ray diffraction, Raman spectroscopy, atomic-force microscopy and piezoelectric switching, we here show that the stripe-like domain patterns result from additional strain imposed on the film when the sample is cooled after growth. At elevated temperature, we determine a transition to a true tetragonal, polar state at 430 °C and we predict a high Curie temperature (T_c ≈ 800 °C). Most importantly, we show that the striped phase is a prerequisite for ferroelectric and piezoelectric switching, which therefore is possible only below ~300 °C, the temperature at which the stripes form. These results show how the delicate interplay between the different strain-stabilized polymorphs of $BiFeO_3$ drives the unique structural and functional properties of this material.

$BiFeO_3$ is the only known material for which strong ferroelectric and magnetic orders coexist at room temperature. The bulk crystal structure is rhombohedral with a remanent polarization of 96 μC/cm^2.[4] Epitaxial films are monoclinically distorted when grown onto substrates that lead to moderately compressive or tensile strains. For films grown on $SrTiO_3$ (i.e. under weak compressive strain) the structure is rhombohedral with a small monoclinic distortion,[7] to distinguish this structure from the bulk rhombohedral (R) phase, it is referred to here as R' (or "R-like"). $BiFeO_3$ can also be stabilized into a monoclinic structure with a large ratio (~1.25) between the out-of-plane (c_{pc}) and the in-plane (a_{pc}, b_{pc}) lattice parameters (where "pc" denotes the pseudocubic notation) when the compressive epitaxial strain exceeds ~4.5%;[3,8] we refer to this polymorph as T' to distinguish it from a true tetragonal (T) structure, noting that terms such as "T-like",[3] "Tri-2",[9] or "M_{II}"[1] are also common in the literature. As we have shown previously,[10] the polymorphic R'-to-T' transformation is also a monoclinic-to-monoclinic R'(M_A)-T'(M_C) structural transition that is part of a R-M_A-M_C-T sequence usually observed only near morphotropic phase boundaries and in lead-based materials [with M_A and M_C being the monoclinic structures corresponding to a $(110)_{pc}$ or $(100)_{pc}$ symmetry plane]. Most striking is the observation that T' films–except at very low film thicknesses–are rarely structurally uniform; instead, a complex array of stripe-like patterns embedded within the T' polymorph emerges. While early work ascribed these patterns to a coexistence between T' and R' (R-like)[3] regions, it is now known that an intermediary polymorph forms, with a *c*-axis lattice parameter close to the midpoint between the R' and T' values. We denote this polymorph S', pointing out that the terms "Tri-1",[9] "M_R"[11] and "M_I"[1] have similarly been used in earlier reports. A careful analysis of the literature shows that scanning-probe induced[2] or electrically driven[12,13] transitions between different polymorphs in $BiFeO_3$ are never between R' and T' (or R and T), but instead always involve this intermediate S' polymorph.[2,14] Therefore, understanding the formation of S' is of paramount importance in the context of this material's functionality.

In this work, we investigate the polymorphic phase transformations between the S' and T' forms of $BiFeO_3$ as well as the structural phase transitions that occur with temperature within the T' polymorph. Specifically, we observe a T'(M_C)-T'(M_A)-T'(T) symmetry change with increasing temperature for $BiFeO_3$ films grown onto $LaAlO_3$ substrates, i.e. a transition from the lower-temperature monoclinic phases to a true tetragonal state, similar to that observed recently for films on $YAlO_3$[15] but until now undetected for films on $LaAlO_3$.[11,14,16] We also find that the S' polymorph, rather than being formed as a consequence of partial strain relaxation during growth, actually forms only at relatively low temperature (after growth) and most likely as a consequence of additional strain caused either by the thermal expansion differences between the film and the substrate[16]

Dr. C. Beekman, Dr. W. Siemons, Dr. T. Z. Ward, Dr. M. Chi, Dr. J. Howe, Dr. H. M. Christen
Materials Science and Technology Division
Oak Ridge National Laboratory
Oak Ridge, TN, 37831, USA
E-mail: christenhm@ornl.gov
Dr. M. D. Biegalski, Dr. N. Balke, Dr. P. Maksymovych
Center for Nanophase Materials Sciences
Oak Ridge National Laboratory
Oak Ridge, TN, 37831, USA
Dr. A. K. Farrar, Dr. J. B. Romero, Prof. D. A. Tenne
Department of Physics
Boise State University
Boise, ID, 83725, USA
Dr. P. Gao, Prof. X. Q. Pan
Department of Materials Science and Engineering
University of Michigan
Ann Arbor, MI, 48109, USA

DOI: 10.1002/adma.201302066

ADVANCED MATERIALS
www.advmat.de

www.MaterialsViews.com

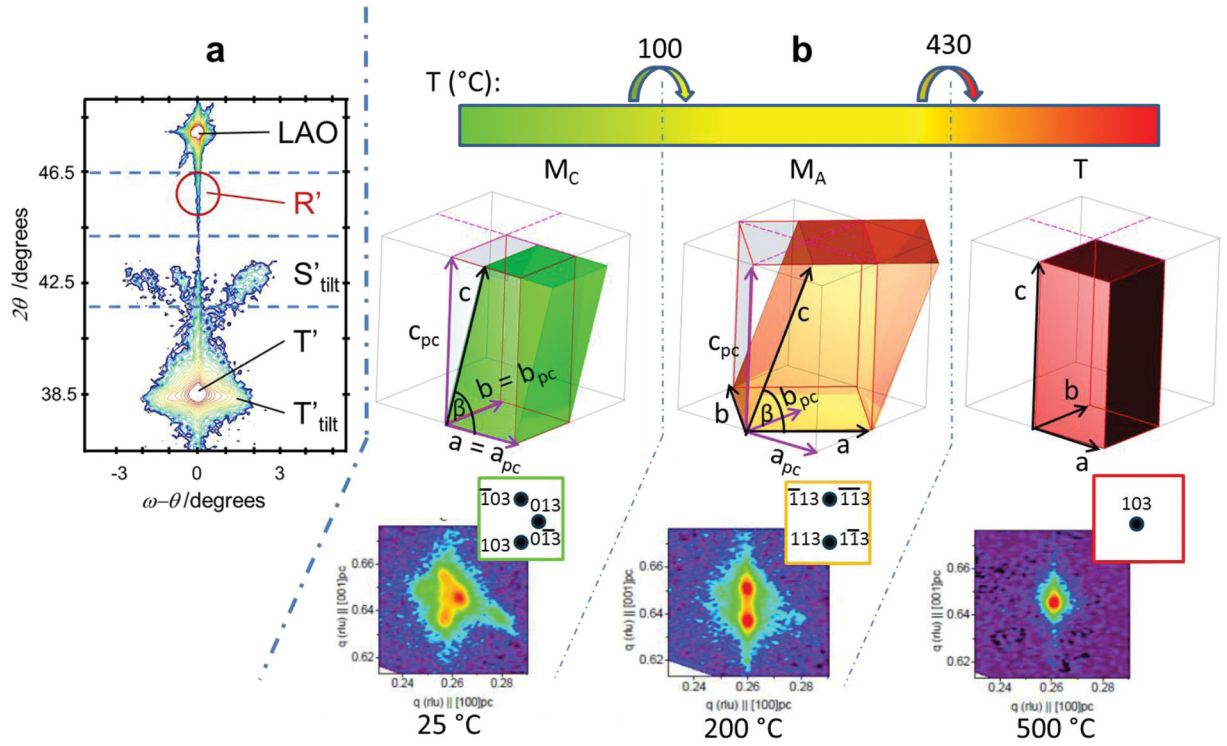

Figure 1. a) Typical X-ray diffraction map $I(\omega\text{-}\theta, 2\theta)$ for a ~45 nm thick $BiFeO_3$ film on a $LaAlO_3$ substrate. The peaks of the $LaAlO_3$ substrate, and the polymorphs of the film (S'_{tilt}, T' and T'_{tilt}) are labeled. The location where the diffraction peak for the R' polymorph would be observed is indicated by a circle. b) Temperature dependence of the structure of the (majority) T' polymorph. (Top) Temperature scale, which indicates the transition temperatures of the structural M_C-M_A-T transition. (Center) Schematic drawing of the monoclinic unit cells with the monoclinic (a, b, c) and pseudocubic (a_{pc}, b_{pc}, c_{pc}) lattice parameters indicated. Shown are the smallest unit cells that are consistent with the data. (Bottom) RSMs through the 103_{pc} family of peaks for the same 45 nm thick $BiFeO_3$ film at $T = 25$ °C (left), $T = 200$ °C (center) and $T = 500$ °C (right). The insets show the indexing of the peaks (using monoclinic indices).

or by an increasing monoclinic distortion as the temperature is lowered. The formation of this polymorph is fully reversible, and its presence is intrinsically linked to the piezoelectric switching in T' $BiFeO_3$: in fact, piezoelectric switching occurs only in the temperature regime where the S' polymorph is observed, i.e. below T~300 °C, but Raman spectroscopy clearly shows that the T' polymorph remains polar at all temperatures investigated.

Epitaxial films of $BiFeO_3$ were grown on $LaAlO_3$ substrates by pulsed-laser deposition as described previously.[10,17] In **Figure 1**a, a typical X-ray diffraction (XRD) map [$I(\omega\text{-}\theta, 2\theta)$] for a ~45 nm thick $BiFeO_3$ film clearly shows the phase coexistence of the S' and T' polymorphs, but the absence of R' in these samples. The majority of the T' phase contributes to a peak aligned with that of the $LaAlO_3$ substrate in ω-scans (indicative of parallel film and substrate (00l) planes). However, a minority component of the T' polymorph and all of S' occur at positions tilted away in ω, in agreement with other reports.[1,9,11] We denote these phases as T'_{tilt} and S'_{tilt}. The origin and functionality of these T'_{tilt} and S'_{tilt} components are discussed in the second half of the paper. First, though, we focus on the strongest polymorph: T'. We use X-ray reciprocal space maps (RSMs) through the 103_{pc} and 113_{pc} family of peaks of a 45 nm thick film to determine the nature of the monoclinic distortion, as in our previous work,[10] but now as function of temperature up to 625 °C. The previously-reported M_C-M_A symmetry change[17] is again observed at ~100 °C, and an additional transition to a true tetragonal structure is detected at 430 °C. Thus, the T' polymorph of $BiFeO_3$ undergoes a temperature-driven sequence of phase transitions T'(M_C)-T'(M_A)-T'(T). This is in agreement with a recent report for films on $YAlO_3$ substrates[15] but thus far has remained undetected in previous work on $LaAlO_3$.[11,14,16] Figure 1b summarizes these transitions and shows representative RSMs containing the 103_{pc} family of peaks, as well as schematic representations of the smallest unit cells consistent with the observed symmetries, as used to index the RSMs. The RSMs taken at different temperatures allow us to determine the in-plane a/b ratio as well as the monoclinic angle β (see Supporting Information Figure S1). Note that neither a/b nor β depend measurably on film thickness t (for 40 nm ≤ t ≤ 100 nm) at any of these temperatures. **Figures 2**a and b show the temperature dependencies of these values. Plotted data are averages obtained from different films with different thickness and/or substrate miscut (see Supporting Information Figure S1). The results show a very clear transition to the tetragonal state at 430 °C (where $a/b = 1$ and $\beta = 90°$).

We now turn our attention to the above-mentioned T'_{tilt} and S'_{tilt} phases and the stripe patterns observed in the films, as visible in the transmission electron

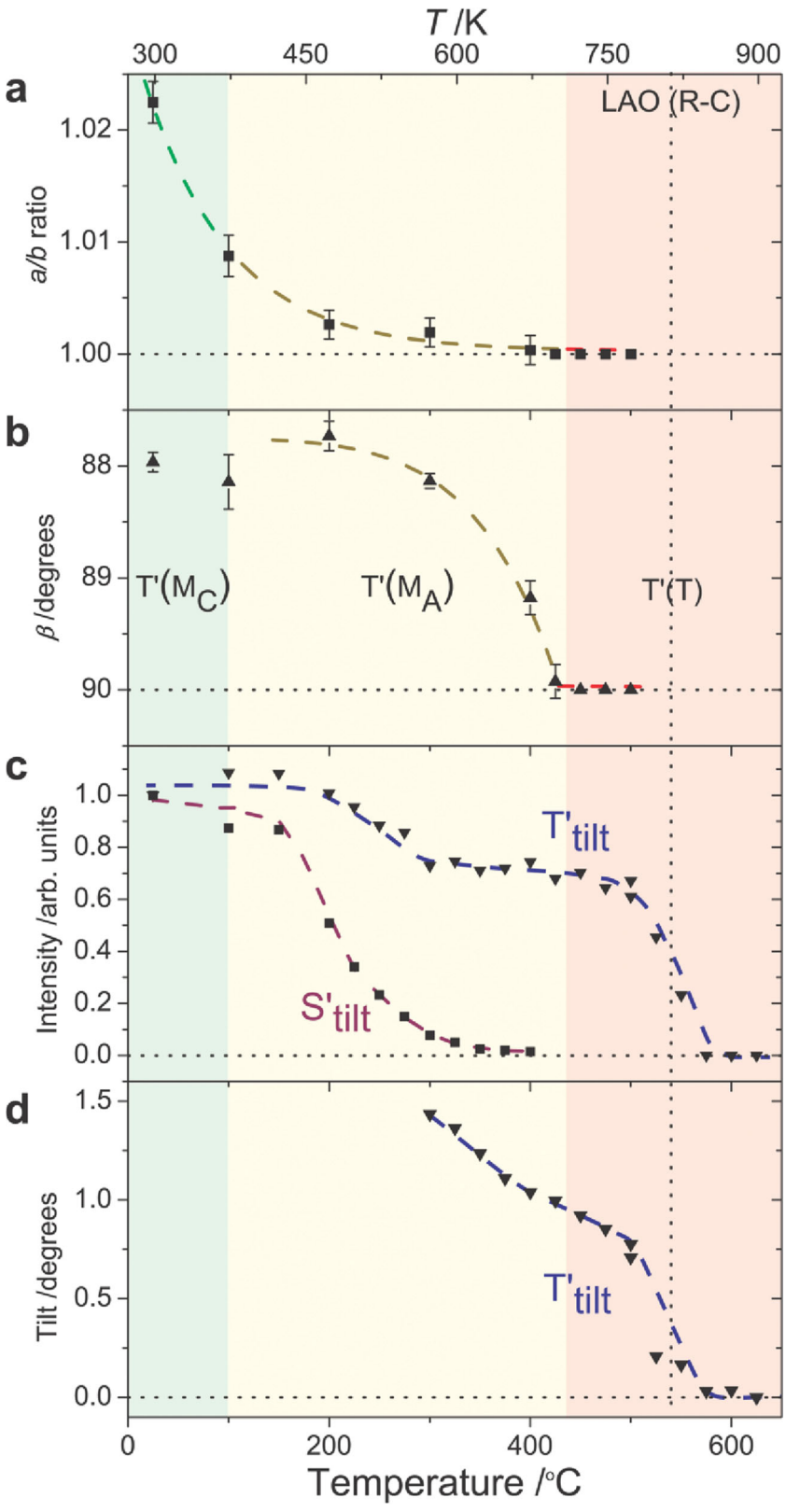

Figure 2. (a) The a/b ratio and (b) the monoclinic angle β as obtained from RSMs through the $BiFeO_3$ peaks for the 103_{pc} and 113_{pc} family of peaks as function of temperature and averaged over multiple films with varying thicknesses (see Supporting Information Figure S1). The dashed lines are power law fits, green for the angles extracted from the 103_{pc} and gold from the 113_{pc} peaks, respectively, the red dashed line is a guide to the eye. The structures of the different phases are indicated. (c) The integrated intensities for the S'_{tilt}-phase (squares) and T'_{tilt} (triangles) 002_{pc} diffraction peaks as extracted from ω-scans as a function of temperature, normalized to the value at room temperature (see Supporting Information Figures S2–S4). The dashed lines are a guide to the eye (S'_{tilt}: purple, T'_{tilt}: blue). (d) Tilt angle of the (00l) planes of the T'_{tilt} polymorph with respect to those of the substrate.

microscopy (TEM) (**Figure 3**) and atomic-force microscopy (AFM) images (**Figure 4**, discussed below) and reported elsewhere previously.[1,3,12–14] Figure 3 shows room-temperature TEM results for cross-section through one of these stripe patterns within a 45 nm thick film. The images confirm the epitaxial alignment between the film and the substrate as well as the high quality of the film/substrate interface. The large-scale dark field image in Figure 3a clearly shows the coexistence of two polymorphs and the resulting impact on the surface morphology, leading to similar slopes as observed previously in AFM investigations.[1,12,18] The different regions are more clearly visible in the high-resolution bright-field image of Figure 3b, where they are indicated by color shades to aid the eye. Selected-area diffraction patterns (Figure 3c–e) are taken from the film (green and sepia), and the substrate (blue). From this, we extract the *c/a* ratio at each location, which allows us to identify the T' and S' polymorphs with $c/a = 1.25$ and 1.09, respectively. This clearly confirms what had been presumed from measurements of the surface angles alone,[1] namely that the phase coexistence regions in highly-strained $BiFeO_3$ consist of the T' and S', but not R' (or R) polymorphs. We also point out the existence of half-integer diffraction peaks in the pattern for the T' structure, indicative of a unit cell doubling within the image plane. This is consistent with the known M_C structure of the T' polymorph and will be investigated in more detail elsewhere. Note that within these stripe patterns, both the T' and S' polymorphs' (00l) planes are tilted with respect to those of the substrate and are thus clearly those leading to XRD scatter intensity at the locations labeled with T'_{tilt} and S'_{tilt} in the X-ray map of Figure 1a.

We monitor the abundance of both the T'_{tilt} and the S'_{tilt} polymorphs as function of temperature (see Figure 2c [squares, S'_{tilt}; triangles, T'_{tilt}]) by determining the integrated intensities as extracted from ω-scans (shown in Supporting Information Figures S2–S4).

ADVANCED MATERIALS
www.advmat.de

Materials Views
www.MaterialsViews.com

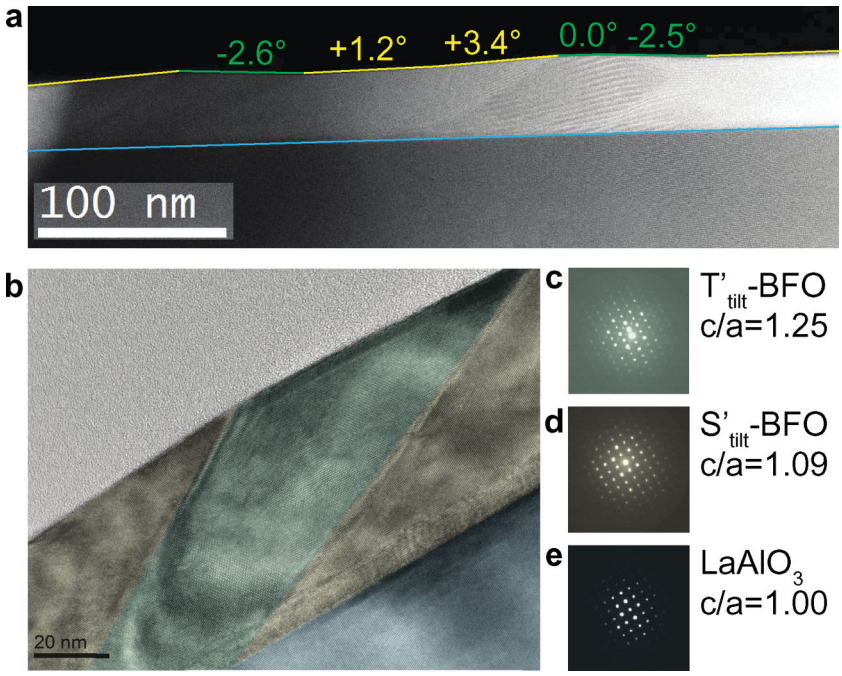

Figure 3. Transmission electron microscopy at room temperature for a 45 nm thick $BiFeO_3$ film grown on a $LaAlO_3$ substrate taken along the 100 zone axis. (a) Dark field scanning TEM image, showing the mixed phase and the angles of the corresponding surface inclination. Scale bar is 100 nm. (b) Colorized bright field high resolution TEM image of film (green and sepia) and substrate (blue). Scale bar is 20 nm. The diffraction patterns correspond to the different phases, (c) T'_{tilt}-phase (green region), (d) S'_{tilt}-phase (sepia region), and (e) $LaAlO_3$ substrate (blue region).

As the film is heated, the intensity of the S'_{tilt}-polymorph starts to strongly decrease around 200 °C, and it fully disappears well below 400 °C. However, the disappearance of the S' polymorph does not coincide with the above-mentioned transition to the true tetragonal state at 430 °C (i.e. where a/b becomes equal to 1). At the same temperature of about 200 °C, the intensity of the T'_{tilt}-polymorph shows a step-wise decrease to a plateau that persists to around 550 °C, well *above* the M_A-T transition. In other words, some of the T'_{tilt} polymorph disappears as S'_{tilt} disappears, consistent with reports that these two phases coexist due to geometric considerations,[1–3,14] but a significant fraction of T'_{tilt} exists independently. In fact, it only disappears at the rhombohedral to cubic structural transition of the $LaAlO_3$ substrate (indicated in Figure 2 by a dotted line at T = 550 °C).[19] In Figure 2d, we show the temperature-evolution of the tilt angle of the T'_{tilt} polymorph. Interestingly, even in the temperature interval from ~300 °C to ~450 °C where its volume fraction (i.e. its integrated X-ray intensity) remains unchanged, the tilt angle monotonically decreases.

The temperature dependent evolution of the phase coexistence is clearly visible in the morphology of the $BiFeO_3$ films. In fact, we have monitored the surface morphology of a 44 nm thick film grown on a 10 nm thick $La_{0.7}Sr_{0.3}MnO_3$ bottom electrode between room temperature and 400 °C. While this bottom electrode is a prerequisite for the subsequent piezoelectric measurements, we note that it does not affect the temperature dependence of the coexistence of the polymorphs or the structural phase transitions of the film. The typical surface morphology at four different temperatures is shown in Figure 4. At room temperature (Figure 4a), the $T'(M_C)$ majority component shows a typical step-and-terrace morphology; embedded within these flat areas are the stripe patterns formed by the S'_{tilt} and T'_{tilt} polymorphs. At intermediate temperatures (Figure 4b, T = 260 °C) the film starts to show a coexistence of two qualitatively different features: the S'_{tilt}/T'_{tilt} stripes as observed at room temperature, and longer single-line features mostly oriented perpendicular to the original S'_{tilt}/T'_{tilt} stripes. Upon further heating (Figure 4c, T = 360 °C), the original S'_{tilt}/T'_{tilt} stripes fully disappear, consistent with the measured temperature dependence of the S'_{tilt} XRD intensity in Figure 2c. However, the longer single lines persist. Finally, in the AFM image taken at T = 400 °C (Figure 4d), the lines are no longer visible.

While more detailed structural characterization is needed to fully understand the nature and evolution of these features, correlating the AFM and XRD data brings us to a clear physical picture: when heated, the S'_{tilt} polymorph disappears much faster than the T'_{tilt} polymorph, which persists to higher temperatures in the form of line features. In other words, at least a portion of the T'_{tilt} polymorph exists independently of the S'_{tilt} polymorph (with which it coexists at low temperature to

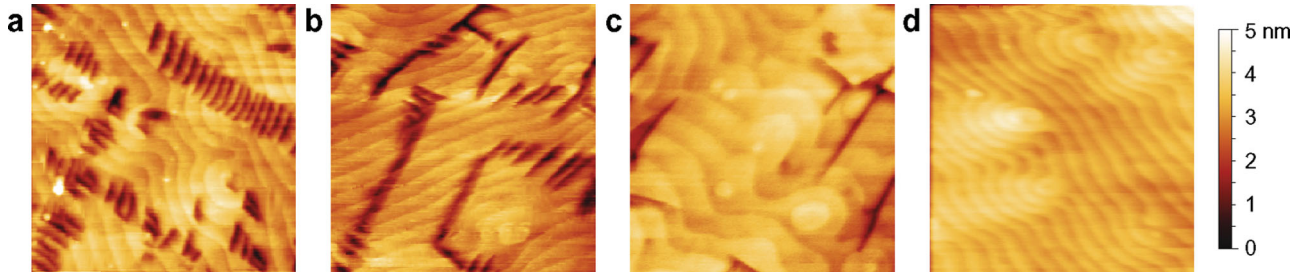

Figure 4. AFM topography images taken at various temperatures (a) T = 25 °C, (b) T = 260 °C, (c) T = 360 °C and (d) T = 400 °C. Scan size = 1.5 µm for all images.

form the stripe patterns). This fraction of the T'$_{tilt}$ polymorph is formed upon cooling through the cubic-to-rhombohedral phase transition of $LaAlO_3$, presumably to accommodate the strain caused by this symmetry lowering. As the corresponding tilt angle decreases with increasing temperature, it becomes less visible in high-temperature AFM images even though XRD clearly indicates its presence. It is probable that the T'$_{tilt}$ lines are the seeding points for the nucleation of the S'$_{tilt}$ polymorph as the sample is cooled below 400 °C. Most importantly, neither the formation of the S' polymorph nor the presence of the T'$_{tilt}$ features are a direct consequence of the structural M_A-T transition. In other words, they both form to accommodate the additional strain imposed by the substrate upon cooling after growth and are not driven directly by the intrinsic phase transitions within T' $BiFeO_3$.

In order to understand the piezoelectric properties of our films we performed piezoresponse force microscopy (PFM) on a $BiFeO_3$ film using a 10 nm $La_{0.7}Sr_{0.3}MnO_3$ film as a bottom electrode. Reversible piezoelectric switching is demonstrated by the out-of-plane phase image recorded after poling with +/− 8 V (see Supporting Information Figure S5). Consistent with results obtained by others, the film is originally poled with a "down" direction of the out-of-plane polarization component but can be switched reversibly. The patterns thus written remain stable for at least several days at room temperature. Note that piezoelectric switching results in a suppression of the S'$_{tilt}$/T'$_{tilt}$ stripe patterns within the switched region and an accumulation thereof along the edges of the poled regions, in agreement with previous results.[2,20] Room temperature displacement loops and additional PFM images are also shown in the Supporting Information Figure S5.

Typical displacement loops were measured at several temperatures. Representative results are shown in **Figure 5**a and show a clear butterfly shape at low and intermediate temperatures, indicating again the reversible piezoelectric switching of the film. Here we note that the magnitude of the piezoresponse and the coercive fields remain unchanged as the sample is heated. However, there are point-to-point variations across the sample, and in fact the probability of a randomly positioned PFM tip landing in a position where the film can be reversibly switched decreases strongly with increasing temperature. In Figure 5b we plot the switching probability as function of temperature. This probability (closed red circles) is determined by monitoring the number of successful loops at each temperature from a set of measurements taken on a grid of 100 positions on the film. Starting at almost a 100% at room temperature, the number of successful loops drops strongly when the film is heated above 200 °C. We find that switching is no longer possible when the film is heated to above 300 °C. In addition to the positions where reversible piezoelectric switching is observed, we find locations for which the loops only show the switching in one bias direction (i.e. polarization switches from down to up, but not back down as the bias polarity is reversed). The probability of recording half loops is low at room temperature but increases upon heating. Its temperature dependence is shown in Figure 5b, where the total success rate of full + half loops is shown as open blue squares. Typical examples of a full and half loop and of a trace for which switching was not measured

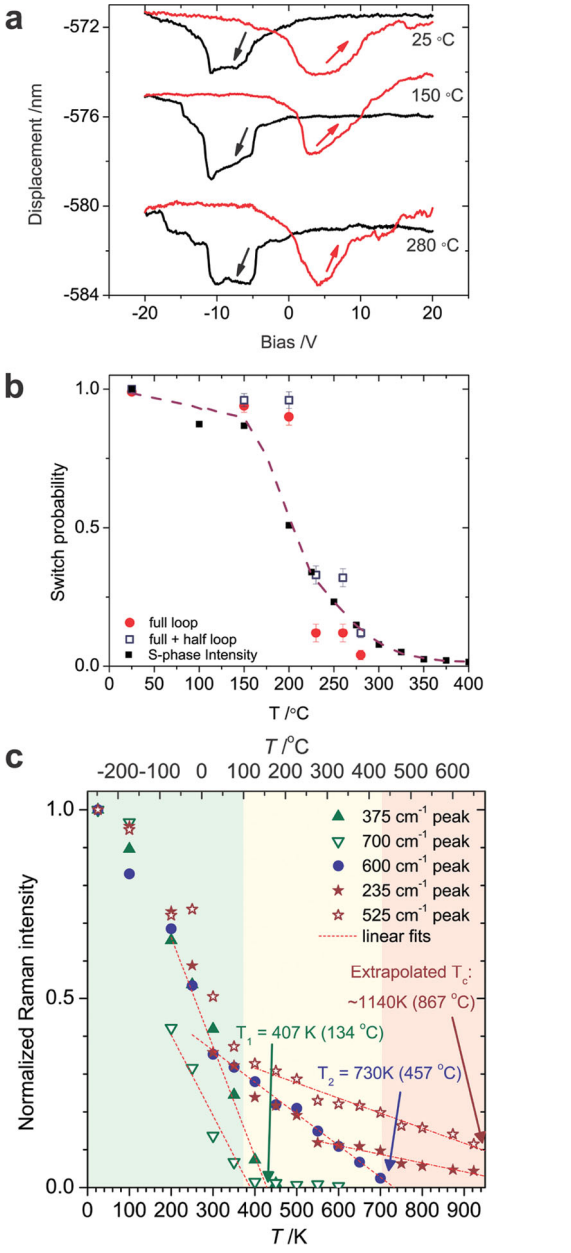

Figure 5. (a) Typical butterfly loops measured at several temperatures taken on a 53 nm thick $BiFeO_3$ film grown on a 10 nm thick $La_{0.7}Sr_{0.3}MnO_3$ bottom electrode. (b) Switching probability as function of temperature (only counting loops that showed fully reversible switching (i.e. full loops), solid red circles; counting both full loops as well as half loops, i.e. loops that only switched from the as-grown down state to the up state (black curves) but not back, open blue squares, see Supporting Information Figure S6 for more details). Integrated intensity for the S'$_{tilt}$ phase (solid black squares) as obtained from XRD measurements is shown for comparison, the purple dashed line is a guide to the eye. (c) Phonon intensities for the phonons at 235, 375, 525, 600 and 700 cm^{-1} as extracted form Raman spectra (see Supporting Information Figure S8) as function of temperature. The dashed lines are linear fits. The transition temperatures are defined as the intercepts of these fits with the abscissa as indicated (T_1 is the average of the intercepts of the modes at 375 and 700 cm^{-1}, T_C is an average of the intercepts of the modes at 235 and 525 cm^{-1}).

are shown in the Supporting Information (Figure S6). In these experiments, upon cooling back from $T > 300$ °C, switching was recovered with the same physical tip and these results were reproduced for multiple thermal cycles. Our results clearly define the temperature range ($T < 300$ °C) for which the film can be switched. To rule out that the switching disappears because the $La_{0.7}Sr_{0.3}MnO_3$ bottom electrode becomes insulating or because the $BiFeO_3$ film becomes too conducting, we first performed lateral resistance measurements as function of temperature on the $La_{0.7}Sr_{0.3}MnO_3$ bottom electrode on a piece of the same film that was used for the switching experiments. As expected, we observe a decrease of resistivity at elevated temperature, i.e., $La_{0.7}Sr_{0.3}MnO_3$ becomes a better electrode material at higher temperature, where switching becomes impossible (see Supporting Information Figure S7a). In particular, the lack of sudden changes is strongly dissimilar from the behavior of the switching probability, and the resistivity changes can, therefore, not explain the switching behavior. In addition, we measured the out-of-plane resistance of the same $BiFeO_3$ film between a macroscopic top Pt electrode and the bottom $La_{0.7}Sr_{0.3}MnO_3$ electrode. The measured resistance gradually decreases with increasing temperature, consistent with the expected insulating behavior (see Supporting Information Figure S7b). Once again, the lack of sudden changes in the resistance behavior clearly indicates that the absence of switching at elevated temperatures is not due to high conductivity of the $BiFeO_3$. Instead, the connection between the presence of the stripes and the switchability of this T'-$BiFeO_3$ is clearly evidenced when we plot the integrated intensity for the S'_{tilt} phase (solid black squares, the purple dashed line is a guide to the eye) as obtained from XRD measurements (see Figure 2c) together with the switching probability (Figure 5b): the drop in switching probability coincides with the decrease in the amount of the striped phase in the film as the film is heated. In other words, the temperature regime for which the film can be switched corresponds to the range in which the S' polymorph exists. This indicates that the presence of the S' polymorph is a prerequisite to piezoelectric switching.

To determine whether the absence of high-temperature piezoelectric switching is a consequence of kinetic barriers (i.e. a lack of a switching path for the polarization) or a consequence of a ferroelectric-paraelectric transition, we turn to Raman spectroscopy as an independent assessment of the polar nature of T' $BiFeO_3$. UV Raman spectroscopy[21] was performed on a 100 nm thick $BiFeO_3$ film as a function of temperature, with results summarized in Figure 5c (see Supporting Information Figure S8 for the raw data). Thinner films yielded qualitatively similar data but a lower signal-to-noise ratio, and were not further investigated. At room temperature, a large number of phonon modes are observed, consistent with the monoclinic nature of $BiFeO_3$. Tracking the temperature-dependent intensity of five of the strongest modes we note that two modes (375 and 700 cm^{-1}) disappear at 134 ± 35 °C (i.e. close to the M_C-M_A transition) and one mode (605 cm^{-1}) at 457 ± 25 °C (i.e. close to the M_C-T transition). Note that the linear fits correspond to a parabolic decrease of displacements with temperature, as Raman intensity is proportional to the square of atomic displacements. At higher temperatures (measured up to 650 °C), two phonon modes (at 235 and 525 cm^{-1}) are still present, very clearly demonstrating that the true tetragonal phase is still polar and therefore, kinetic barriers are most likely the origin of reduced switching at higher temperatures. A linear fit predicts these peaks' disappearance at 867 ± 100 °C, which we take as an estimate of the Curie temperature of T' $BiFeO_3$. Therefore, T' $BiFeO_3$ likely exhibits a Curie temperature fairly close to that of R' films ($T_c \approx 760$ °C).[22]

In conclusion, our temperature dependent studies of highly strained $BiFeO_3$ films yield a detailed description of their structural and piezoelectric properties. Our data show a transition to a true tetragonal high-temperature state at 430 °C; this tetragonal phase is polar with an estimated Curie temperature above 800 °C. However, piezoelectric (and thus, by extension, ferroelectric) switching is only possible at much lower temperatures (below ≈ 300 °C), as it requires the presence of or the ability to form the additional S' polymorph. Our results clearly indicate that this S'-$BiFeO_3$ forms upon cooling as a consequence of additional strain imposed on the film and not as a partial strain relaxation during growth. This leads to the formation of the S'_{tilt}/T'_{tilt} stripe patterns; however, a portion of the T'_{tilt} polymorph already forms at the cubic-to-rhombohedral phase transition of the $LaAlO_3$ substrate. Understanding the nature of the coexistence of these multiple polymorphs in highly strained $BiFeO_3$ and their role in ferroelectric and piezoelectric switching will aid in tuning the functional properties of $BiFeO_3$ for specific applications, and broaden our understanding of materials that are close to strain-induced morphotropic phase boundaries.

Experimental Section

Film growth: The experiments were performed on films of $BiFeO_3$ grown on $LaAlO_3$ substrates by pulsed laser deposition (PLD). The films were grown in a vacuum system with a base pressure of 5×10^{-7} Torr in a 25 mTorr oxygen background pressure while the substrate was kept at a temperature of 675 °C. A pulsed KrF excimer laser with a wavelength of 248 nm was focused on a 10% excess Bi $BiFeO_3$ sintered pellet with an energy density of 0.4 J/cm^2 and operated at 2 Hz, resulting in an average deposition rate of ~0.03 Å/pls.

X-ray diffraction: The crystal structure was investigated using a X-ray diffractometer (PanAlytical X'Pert MRD Pro) with Cu $K_{\alpha 1}$ radiation. To perform the experiments at elevated temperatures, we used a high temperature stage (DHS-900) with a dome over the sample, allowing a flow of oxygen during heating.

AFM: Room-temperature AFM micrographs were taken on a Veeco D3100 operated in tapping mode. Temperature dependence of the surface topography and piezoelectric displacement loops was measured in ultrahigh vacuum using an Omicron VT-SPM modified for piezoresponse force microscopy.[23] The $BiFeO_3$ film was attached to a tantalum foil, which was subsequently clamped against a PBN heater in a special sample holder. Sample temperatures quoted in the text were obtained from a separate calibration of the temperature of the tantalum foil (measured by a miniature thermocouple) versus the heater current. All the vacuum experiments were carried out at pressures better than 5×10^{-9} Torr using Pt-coated conducting AFM tips (Budget Sensors ElectriMulti75). No substantial surface degradation was observed after one, and even several temperature cycles. To assure self-consistency, piezoelectric properties were measured at room temperature before and after the heating cycle.

Room temperature PFM: The PFM measurements were performed on a Veeco Dimension Nanoscope 5 AFM equipped with external lock-in amplifiers. Using conducting AFM tips we measured the local electrical and topographical properties simultaneously and independently. For

PFM imaging, a single frequency ac bias of 2V close to the contact resonance frequency of the tip-sample contact was applied to the tip and the PFM amplitude and phase were recorded. For poling, a dc voltage of +/− 8V was applied to the scanning tip which was sufficient to reverse the orientation of the ferroelectric domains without inducing topographic changes (i.e. sample destruction).

TEM: The TEM characterization was carried out on an FEI-Titan 60/300 microscope at the operation voltage of 300 kV. TEM specimens were prepared using mechanical polishing, followed by low-voltage (2 kV) cryo ion-milling.

Raman spectroscopy: Raman spectra of $BiFeO_3$ films were measured in backscattering geometry normal to the film surface using a Jobin Yvon T64000 triple spectrometer equipped with a liquid nitrogen cooled multichannel charge coupled device detector. An ultraviolet excitation (325 nm line of He-Cd laser) was used for excitation in order to reduce the substrate contribution.[21] Maximum laser power density was ≈0.5 W/mm^2 at the sample surface, low enough to avoid any noticeable local heating of the sample.[21] Spectra were recorded in the temperature range 10–950 K using a variable temperature closed cycle helium cryostat and a high-temperature stage (Supporting Information, Figure S8).

Supporting Information

Supporting Information is available from the Wiley Online Library or from the author.

Acknowledgements

Research supported in part by the U.S. Department of Energy (DOE), Basic Energy Sciences (BES), Materials Sciences and Engineering Division (authors C.B., W.S., T.Z.W., J.H., and H.M.C.: film growth, XRD, AFM, PFM) and the Scientific User Facilities Division (author M.C.: TEM). User projects were supported at ORNL's Shared Research Equipment (ShaRE) User Program (SEM) and the Center for Nanophase Materials Research (CNMS, high-temperature XRD, AFM, PFM), which are both also sponsored by DOE-BES. Raman studies at Boise State University were supported by NSF under grant DMR-1006136. Initial electron microscopy work performed at the University of Michigan was supported by the Department of Energy (DOE) under the grant DE-FG02-07ER46416 and by the National Science Foundation under DMR-0820404 (PG) and DMR-0723032 (TEM instrument).

Received: May 7, 2013
Published online: July 12, 2013

[1] A. R. Damodaran, C. W. Liang, Q. He, C. Y. Peng, L. Chang, Y. H. Chu, L. W. Martin, *Adv. Mater.* **2011**, *23*, 3170.
[2] Y. C. Chen, Q. He, F. N. Chu, Y. C. Huang, J. W. Chen, W. I. Liang, R. K. Vasudevan, V. Nagarajan, E. Arenholz, S. V. Kalinin, Y. H. Chu, *Adv. Mater.* **2012**, *24*, 3070.
[3] R. J. Zeches, M. D. Rossell, J. X. Zhang, A. J. Hatt, Q. He, C.-H. Yang, A. Kumar, C. H. Wang, A. Melville, C. Adamo, G. Sheng, Y.-H. Chu, J. F. Ihlefeld, R. Erni, C. Ederer, V. Gopalan, L. Q. Chen, D. G. Schlom, N. A. Spaldin, L. W. Martin, R. Ramesh, *Science* **2009**, *326*, 977.
[4] A. J. Hatt, N. A. Spaldin, C. Ederer, *Phys. Rev. B* **2010**, *81*, 54109.
[5] M. D. Rossell, R. Erni, M. P. Prange, J.-C. Idrobo, W. Luo, R. J. Zeches, S. T. Pantelides, R. Ramesh, *Phys. Rev. Lett.* **2012**, *108*, 047601.
[6] J. X. Zhang, Q. He, M. Trassin, W. Luo, D. Yi, M. D. Rossell, P. Yu, L. You, C. H. Wang, C. Y. Kuo, J. T. Heron, Z. Hu, R. J. Zeches, H. J. Lin, A. Tanaka, C. T. Chen, L. H. Tjeng, Y.-H. Chu, R. Ramesh, *Phys. Rev. Lett.* **2011**, *107*, 147602.
[7] H. W. Jang, D. Ortiz, S. H. Beak, C. M. Folkman, R. R. Dias, P. Schafer, Y. B. Chen, C. T. Nelson, X. Q. Pan, R. Ramesh, C. B. Eom, *Adv. Mater.* **2009**, *21*, 817.
[8] H. Béa, B. Dupé, S. Fusil, R. Mattana, E. Jacquet, B. Warot-Fonrose, F. Wilhelm, A. Rogalev, S. Petit, V. Cros, A. Anane, F. Petroff, K. Bouzehouane, G. Geneste, B. Dkhil, S. Lisenkov, I. Ponomareva, L. Bellaiche, M. Bibes, A. Barthélémy, *Phys. Rev. Lett.* **2009**, *102*, 217603.
[9] Z. H. Chen, S. Prosandeev, Z. L. Luo, W. Ren, Y. J. Qi, C. W. Huang, L. You, C. Gao, I. A. Kornev, T. Wu, J. L. Wang, P. Yang, T. Sritharan, L. Bellaiche, L. Chen, *Phys. Rev. B* **2011**, *84*, 094116.
[10] H. M. Christen, J. H. Nam, H. S. Kim, A. J. Hatt, N. A. Spaldin, *Phys. Rev. B* **2011**, *83*, 144107.
[11] J. Kreisel, P. Jadhav, O. Chaix-Pluchery, M. Varela, N. Dix, F. Sanchez, J. Fontcuberta, *J. Phys. Condens. Mat.* **2011**, *23*, 342202.
[12] J. Zhou, M. Trassin, Q. He, N. Tamura, M. Kunz, C. Cheng, J. X. Zhang, W. I. Liang, J. Seidel, C. L. Hsin, J. Q. Wu, *J. Appl. Phys.* **2012**, *112*, 064102.
[13] D. Mazumdar, V. Shelke, M. Iliev, S. Jesse, A. Kumar, S. V. Kalinin, A. P. Baddorf, A. Gupta, *Nano Lett* **2010**, *10*, 2555.
[14] H. J. Liu, C. W. Liang, W. I. Liang, H. J. Chen, J. C. Yang, C. Y. Peng, G. F. Wang, F. N. Chu, Y. C. Chen, H. Y. Lee, L. Chang, S. J. Lin, Y. H. Chu, *Phys. Rev. B* **2012**, *85*, 014104.
[15] H. J. Liu, H. J. Chen, W. I. Liang, C. W. Liang, H. Y. Lee, S. J. Lin, Y. H. Chu, *J. Appl. Phys.* **2012**, *112*, 052002.
[16] C. J. C. Bennett, H. S. Kim, M. Varela, M. D. Biegalski, D. H. Kim, D. P. Norton, H. M. Meyer, H. M. Christen, *J. Mater. Res.* **2011**, *26*, 1326.
[17] W. Siemons, M. D. Biegalski, J. H. Nam, H. M. Christen, *Appl. Phys. Express* **2011**, *4*, 095801.
[18] Q. He, Y. H. Chu, J. T. Heron, S. Y. Yang, W. I. Liang, C. Y. Kuo, H. J. Lin, P. Yu, C. W. Liang, R. J. Zeches, W. C. Kuo, J. Y. Juang, C. T. Chen, E. Arenholz, A. Scholl, R. Ramesh, *Nat. Commun.* **2011**, *2*, 1.
[19] S. A. Hayward, S. A. T. Redfern, E. K. H. Salje, *J. Phys. Condens. Mat.* **2002**, *14*, 10131.
[20] K. T. Ko, M. H. Jung, Q. He, J. H. Lee, C. S. Woo, K. Chu, J. Seidel, B. G. Jeon, Y. S. Oh, K. H. Kim, W. I. Liang, H. J. Chen, Y. H. Chu, Y. H. Jeong, R. Ramesh, J. H. Park, C. H. Yang, *Nat. Commun.* **2011**, *2*, 225.
[21] D. A. Tenne, A. Bruchhausen, N. D. Lanzillotti-Kimura, A. Fainstein, R. S. Katiyar, A. Cantarero, A. Soukiassian, V. Vaithyanathan, J. H. Haeni, W. Tian, D. G. Schlom, K. J. Choi, D. M. Kim, C. B. Eom, H. P. Sun, X. Q. Pan, Y. L. Li, L. Q. Chen, Q. X. Jia, S. M. Nakhmanson, K. M. Rabe, X. X. Xi, *Science* **2006**, *313*, 1614.
[22] H. Toupet, F. Le Marrec, C. Lichtensteiger, B. Dkhil, M. G. Karkut, *Phys. Rev. B* **2010**, *81*, 140101(R).
[23] P. Maksymovych, S. Jesse, M. Huijben, R. Ramesh, A. Morozovska, S. Choudhury, L.-Q. Chen, A. P. Baddorf, S. V. Kalinin, *Phys. Rev. Lett.* **2009**, *102*, 017601.